



Improvements of the Longitudinal Magnetic Field Measurement from the *Solar Magnetic Field Telescope* at the Huairou Solar Observing Station

Andrei Plotnikov^{1,2} · Alexander Kutsenko^{1,2} · Shangbin Yang¹ · Haiqing Xu¹ · Xianyong Bai¹ · Hongqi Zhang¹ · Kirill Kuzanyan³

Received: 30 July 2020 / Accepted: 20 September 2021 / Published online: 15 November 2021
© The Author(s), under exclusive licence to Springer Nature B.V. 2021

Abstract

The weak-field approximation, implying a linear relationship between Stokes- V/I and the longitudinal magnetic field [B_{\parallel}], often suffers from saturation observed in strong magnetic-field regions such as sunspot umbrae. In this work, we seek to improve the magnetic-field observations carried out by the *Solar Magnetic Field Telescope* (SMFT) at the Huairou Solar Observing Station, China. We propose using a non-linear relationship between Stokes- V/I and B_{\parallel} to derive the magnetic field. To determine the form of the relationship, we perform a cross-calibration of the observed SMFT data and magnetograms provided by the *Helioseismic and Magnetic Imager* onboard the *Solar Dynamics Observatory*. The algorithm for the magnetic-field derivation is described in detail. We show that using a non-linear relationship between Stokes- V/I and B_{\parallel} allows us to eliminate magnetic-field saturation inside the sunspot umbra. The proposed technique enables one to enhance the reliability of the SMFT magnetic-field data obtained even long before the space-based instrumentation era, since 1987.

Keywords Magnetic fields, photosphere · Instrumentation and data management · Instrumental effects

1. Introduction

The *Solar Magnetic Field Telescope* (SMFT) is a narrow-band filtergraph installed at the Huairou Solar Observing Station (HSOS), the National Astronomical Observatories, Chinese Academy of Sciences (Ai, 1987). The field-of-view of the telescope is $225'' \times 170''$. The pixel size of the acquired filtergrams is $0.295'' \times 0.287''$ while the spatial resolution of about

✉ A. Plotnikov
plotnikov.andrey.alex@yandex.ru

¹ Key Laboratory of Solar Activity, National Astronomical Observatories of China, Chinese Academy of Sciences, Beijing, 100101, China

² Crimean Astrophysical Observatory, Russian Academy of Sciences, Nauchny, Crimea, 298409, Russia

³ IZMIRAN, Russian Academy of Sciences, Troitsk, Moscow, 108840, Russia

$2''$ is limited by atmospheric seeing. The telescope operation of SMFT provides a continuous, homogeneous observational data set on the solar vector magnetic field since 1987. Such a long, unique data series allows one to analyze long-term variations and solar-cycle dependence of active-region parameters that rely on the vector magnetic-field measurements, for example, the current helicity of active regions (e.g. Zhang et al., 2010). SMFT uses the photospheric Fe I 5324.19 Å spectral line to derive information on solar magnetic fields. Stokes- $(V/I)_{\text{SMFT}}$ is routinely measured at a single wavelength in the wing of the spectral line ($\approx 75 \text{ mÅ}$ from the line center).

The magnetic field is traditionally obtained in the framework of the weak-field approximation, implying a linear relationship between the measured Stokes $(V/I)_{\text{SMFT}}$ and longitudinal magnetic field $[B_{\parallel}]$:

$$B_{\parallel} = C_{\parallel} \frac{V}{I}. \quad (1)$$

The calibration coefficient $[C_{\parallel}]$ for HSOS/SMFT measurements was analytically obtained for the first time by Ai, Li, and Zhang (1982). Several other methods for weak-field calibration have been proposed recently (see Bai, Deng, and Su, 2013, and references therein).

In fact, the linear relationship between Stokes- V/I and the longitudinal magnetic field B_{\parallel} holds as long as the magnetic field does not exceed a certain value that depends on many factors. As we will show below, this value is about 1000 G for SMFT. For stronger magnetic fields, which are readily observed in the umbrae of sunspots, Stokes- V/I decreases with increasing $[B_{\parallel}]$ (e.g. Sakurai et al., 1995) resulting in significant underestimation of the sunspot umbra magnetic field. It is worth noting that the deviation from the linear relationship between Stokes- V/I and the longitudinal magnetic field B_{\parallel} is also caused by different solar atmosphere conditions (e.g. Zhang, 2019). Thus, the quiet-Sun areas and the umbral regions exhibit different magnetic sensitivity due to temperature differences. The ratio between the Stokes- V/I measured for the quiet-Sun and within the umbra regions may reach 1.8 for the Fe I 5324.19 Å spectral line (Zhang, 2019).

The reliability of the transverse magnetic-field measurements also depends to a great extent on the measurements of the longitudinal magnetic field. The reason for this is the so-called 180-degree ambiguity problem, when the azimuthal direction of the transverse magnetic-field vector cannot be directly determined from the observations. A number of techniques have been proposed to solve this ambiguity (e.g. Metcalf, 1994). Most of these techniques use the observed longitudinal magnetic field to calculate the configuration of the potential field. Then, the observed transverse magnetic field is directed along the potential transverse field (e.g. Canfield et al., 1993). Other methods may use various criteria to perform the disambiguation. However, it is worth noting that the disambiguation procedure relies exclusively on a number of physical assumptions. Calculations of the electric currents imply deriving the spatial derivative of the transverse magnetic field. In such a case, the magnitude, sign, and spatial structure of the electric currents and the current helicity depend strongly on the correct 180-degree disambiguation of the transversal magnetic field. In the case of longitudinal magnetic-field saturation inside a sunspot, the 180-degree disambiguation procedure may turn the azimuthal component of the transverse magnetic field in the wrong direction, resulting in incorrect estimation of the electric currents and, consequently, the current helicity.

The saturation problem might be solved by applying state-of-the-art machine-learning techniques. Thus, recently Guo et al. (2020) developed an approach for non-linear calibration of filter-based magnetographs. The approach employs a trained multilayer perceptron

aimed at deriving magnetic-field parameters from Stokes- I , $-Q$, $-U$, and $-V$ measured at a single wavelength. However, the method has yet be adopted for HSOS/SMFT data.

Saturation of the longitudinal magnetic field inside a sunspot can be eliminated by using additional information on the spectral line, i.e. when the data on spectral-line profile are available. Thus, Bai et al. (2014) derived the magnetic-field vector by fitting six points of the Fe I 5324.19 Å spectral-line profile with analytical Stokes profiles obtained in the Milne–Eddington (ME) atmosphere approximation. A similar procedure was applied by Su and Zhang (2004) who used 31 points of the same spectral-line profile to derive the vector magnetic field. See Section 2 for more details on the magnetic field deriving from the observed Stokes vector. The longitudinal magnetic field can also be derived by a more rapid and straightforward center-of-gravity method (Rees and Semel, 1979): B_{\parallel} is proportional to the difference of the centers of gravity of spectral lines in the right- and left-circular polarization states.

However, routine measurements of Stokes- $(V/I)_{\text{SMFT}}$ by HSOS/SMFT are performed at a single wavelength point of the Fe I 5324.19 Å spectral-line profile. In this article, we make an attempt to improve routine magnetic-field measurements by introducing a non-linear relationship between the Stokes- $(V/I)_{\text{SMFT}}$ and the longitudinal magnetic field.

2. Theoretical Background

Polarization of the light emitted by the solar atmosphere emerges as a result of the radiation propagation through a magnetized plasma. The resultant state of the light is described by the wavelength-dependent Stokes pseudo-vector $\mathbf{I} = (I, Q, U, V)$, where I is the total intensity, Q and U are the components associated with linear polarization, and V is the component attributed to circular polarization. The Stokes profiles, which are determined by physical parameters of the atmosphere, can be derived by solving the radiative-transfer equation (RTE) for a certain atmosphere model. However, in practice, the observables are four spectral profiles of the Stokes-vector components $I(\lambda)$, $Q(\lambda)$, $U(\lambda)$, $V(\lambda)$. Therefore, one has to solve the inverse problem to infer the magnetic-field and thermodynamical parameters of the medium that the light propagates through (see, e.g. del Toro Iniesta and Ruiz Cobo, 2016). A description of currently used techniques and approaches used to inverse the Stokes profiles can be found in the review by del Toro Iniesta and Ruiz Cobo (2016).

The RTE can be expressed in the form (e.g. del Toro Iniesta, 2003)

$$\frac{d\mathbf{I}}{d\tau_c} = \mathbf{K}(\mathbf{I} - \mathbf{S}), \quad (2)$$

where τ_c is the optical depth at the continuum wavelength, \mathbf{K} is the propagation matrix, and \mathbf{S} is the source function. The propagation matrix \mathbf{K} describes energy absorption, injection, and transfer between different polarization states (e.g. del Toro Iniesta and Ruiz Cobo, 2016). Elements of the propagation matrix are combinations of Voigt and Faraday–Voigt functions. In general, the propagation matrix \mathbf{K} and the source function \mathbf{S} depend on the optical depth.

The inversion of the RTE requires the numerical solution of a set of integral equations. This problem requires a lot of resources when one considers a stratified atmosphere that is in a non-local-thermodynamic equilibrium state. However, for certain special cases there is an analytical solution. One of the most widely used simplifications is the ME atmosphere. ME assumes that propagation matrix is independent of optical depth and the source function depends linearly on optical depth, i.e. ME is applicable to a certain extent for photospheric line

analysis. In this case, the RTE has an analytical solution known as the Unno–Rachkovsky solution (Unno, 1956; Rachkovsky, 1962). The four Stokes profiles are determined by nine parameters, namely three components of the magnetic field (field strength, inclination, and azimuth), the line-of-sight velocity of the plasma, the Doppler width of the spectral line, the line-to-continuum absorption coefficient, the damping parameter, the source function, and the source function's gradient. For instance, the ME approximation is used to infer solar vector magnetic fields and Doppler velocities from Stokes-vector observations (Borrero et al., 2011) taken by the *Helioseismic and Magnetic Imager* onboard the *Solar Dynamics Observatory* (SDO/HMI: Scherrer et al., 2012; Schou et al., 2012).

When the longitudinal magnetic field is weak and the Zeeman splitting of the line is much smaller than the Doppler width, the Voigt and Faraday–Voigt functions in the propagation matrix \mathbf{K} can be replaced by the lower-order terms of its Taylor series (Landi Degl'Innocenti and Landi Degl'Innocenti, 1973; Jefferies, Lites, and Skumanich, 1989). In such a case, assuming that the atmosphere is in local thermodynamic equilibrium, the RTE can be further simplified. Landi Degl'Innocenti and Landolfi (2004) showed that for the weak magnetic-field regime the following relationship holds (we use the notation from del Toro Iniesta and Ruiz Cobo, 2016):

$$V(\lambda) = -g_{\text{eff}} \Delta\lambda_B \cos \gamma \frac{\partial I_{\text{nm}}}{\partial \lambda}, \quad (3)$$

where g_{eff} is the effective Landé factor, γ is inclination, I_{nm} is the Stokes- I profile in the absence of magnetic field, and the Zeeman splitting

$$\Delta\lambda_B = \frac{\lambda_0^2 e_0 B}{4\pi mc^2}. \quad (4)$$

In Equation 4, λ_0 is the central wavelength of the spectral line, c is the speed of light, e_0 and m are electron's charge and mass, respectively. By substituting Equation 4 into Equation 3, one can easily obtain the magnetograph formula (Equation 1). The weakness of the magnetic field implies

$$g_{\text{eff}} \frac{\Delta\lambda_B}{\Delta\lambda_D} \ll 1, \quad (5)$$

where $\Delta\lambda_D$ is the Doppler width of the spectral line. However, the weak-field approximation is not valid for stronger magnetic fields: higher-order terms in the Taylor series of Voigt and Faraday–Voigt functions in the propagation matrix start to play a significant role as the magnetic-field strength increases. del Toro Iniesta and Ruiz Cobo (2016) argued that the saturation of Stokes- V/I can be seen even for relatively weak magnetic fields of about several hundreds of gauss.

The Fe I 5324 Å spectral line used in HSOS/SMFT exhibits relatively large total width. One should expect the weak-field approximation to be valid over a broad range of magnetic-field strengths. The theoretical relationship between the Stokes- V/I and longitudinal magnetic field for the Fe I 5324 Å spectral line was investigated in Ai, Li, and Zhang (1982) and in Su and Zhang (2004), and we refer the reader to these articles for details.

In this work we have also carried out the simulation of the saturation of the Stokes- V/I in the weak-field regime for Fe I 5324 Å. The results are shown in the left panel of Figure 1. The Stokes- V and $-I$ profiles were calculated using the SIR code (Cobo and del Toro Iniesta, 1992; Bellot Rubio, 2003). To roughly imitate filtergraph observations, the Stokes-vector profiles were sampled at a single wavelength position shifted by 75 mÅ from the line

center. The blue curve in the left panel of Figure 1 was derived by using atmospheric parameters provided by the semi-empirical FALC model (Fontenla, Avrett, and Loeser, 1993). The model describes the quiet-Sun atmosphere; therefore, the left-hand (weak-field) part of the blue curve is supposed to be valid. The orange curve in the left panel of Figure 1 was obtained using atmospheric parameters from the MACKKL model by Maltby et al. (1986). The latter model describes the thermodynamics of sunspot umbrae. Hence, this model could be more suitable for the strong-field part of the Stokes- V/I versus B_{\parallel} relationship. One can see that the curves have different slopes. In our opinion, simulation of the exact behavior of Stokes- V/I versus B_{\parallel} in the weak-field regime requires more sophisticated atmospheric models that take into account the changes of the atmosphere thermodynamic as one switches from weak quiet-Sun magnetic fields to strong magnetic field inside sunspot umbra. Besides that, the shape of the relationship also depends on other factors, e.g. the inclination of the magnetic-field vector (see, e.g., Figure 11.1 of Landi Degl'Innocenti and Landolfi, 2004).

The reason for the Stokes- V/I saturation in the weak-field approximation can be easily seen in the right panel of Figure 1. The colored curves show simulated Stokes- V/I profile (in the framework of the ME atmosphere approximation) for several values of the magnetic-field strength (the vector of the magnetic field is supposed to be co-aligned with the line-of-sight). The vertical black line denotes the central position of a filter in the wing of the spectral line. One can see that for weak magnetic fields the Stokes- V/I sampled at the filter position gradually increases with the magnetic field. As the magnetic field grows, the peaks of the V/I -profile shift farther from the spectral-line center, resulting in saturation and further decrease in sampled V/I .

The saturation can be explained in a more simplified qualitative way. It is the Zeeman splitting of the spectral line, i.e. the displacement of the polarized component of the spectral line from the unperturbed-wavelength position, which is proportional to the magnetic-field strength (Equation 4). When the magnetic field is weak, the amplitude of the Stokes- V/I is roughly proportional to the displacement. As the magnetic-field strength increases, the amplitude of the Stokes- V/I reaches a certain saturated value (the relationship $I^2 \geq Q^2 + U^2 + V^2$ holds) and shifts farther from the line center. Hence, in order to overcome the saturation, one has to use the information on the Stokes profile to determine the splitting itself. Therefore, inversion techniques such as those based on ME approximation or more sophisticated atmospheric models require several (more than two) wavelength points of the Stokes profiles as input data. At the same time, as stated by del Toro Iniesta and Ruiz Cobo (2016), the magnetograph formula (Equation 1) is the only way to get information on the longitudinal magnetic field if the instrument samples the circular polarization at one or two wavelength positions.

3. The Method

To establish the relationship between the HSOS/SMFT Stokes- $(V/I)_{\text{SMFT}}$ and the longitudinal magnetic field $[B_{\text{SMFT}}]$ we performed a cross-calibration of Stokes- $(V/I)_{\text{SMFT}}$ and the longitudinal magnetic field B_{HMI} provided by SDO/HMI. SDO/HMI is a full-disk filtergraph that measures the profile of the photospheric Fe I 6173 Å line at six wavelength positions in various polarization states to derive the information on four spectral profiles of the Stokes vector. The spatial resolution of the instrument is approximately 1.5'' with 0.5'' × 0.5'' pixel size.

A ME-based Very Fast Inversion of the Stokes Vector code (VFISV), described in detail by Borrero et al. (2011), is used to process SDO/HMI pipeline data and derive the vector

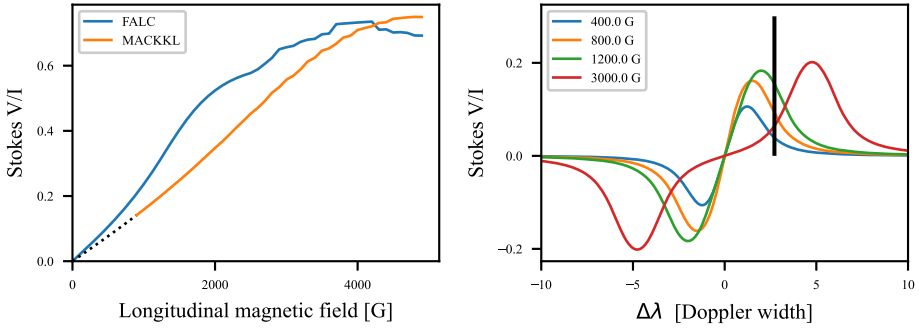


Figure 1 Left – Stokes- V/I versus longitudinal magnetic-field relationship for the Fe I 5324 Å spectral line. Stokes- V/I is supposed to be sampled in the wing of the spectral line. The relationship was calculated using the SIR code. The atmospheric thermodynamics parameters were retrieved from the FALC (blue curve) and MACKKL (orange curve) semi-empirical atmospheric models. The MACKKL model is applicable for sunspot umbrae, therefore the distribution for magnetic fields below 1000 G is plotted by a dashed line. Right – Simulated Stokes- (V/I) profiles for several magnetic-field strength values. The calculations were performed in the framework of the ME approximation. The black vertical line shows the plausible tuning position of the filter used to sample Stokes- V/I . The reason of the saturation in the weak-field approximation is clearly seen. In both panels the magnetic field is co-aligned with the line-of-sight.

magnetic field. The magnetic-field maps of active regions are available in the form of patches of full-disk maps (Bobra et al., 2014; Hoeksema et al., 2014). These patches were used to perform cross-calibration with the HSOS/SMFT observations. The SDO/HMI longitudinal magnetic field was derived as $B_{\text{HMI}} = B_{\text{HMI}}^{\text{strength}} \cos(B_{\text{HMI}}^{\text{incl}})$, where $B_{\text{HMI}}^{\text{strength}}$ and $B_{\text{HMI}}^{\text{incl}}$ are the magnetic-field strength and inclination, respectively.

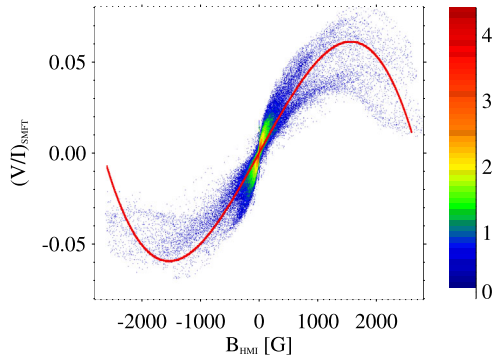
For cross-calibration we used co-temporal magnetograms of ten randomly selected active regions observed between 2015 and 2018. The magnetograms acquired by SDO/HMI were rotated by the p -angle and rescaled to the pixel size of HSOS/SMFT of approximately $0.29'' \times 0.29''$ by a cross-correlation technique. Since the SDO/HMI data are not affected by seeing, the magnetograms from the space-borne instrument were smoothed by a 2D Gaussian kernel of $1.5'' \times 1.5''$ to roughly imitate the atmospheric blurring. Then, the same regions of the solar surface were cropped from the processed SDO/HMI magnetograms and from the HSOS/SMFT Stokes- $(V/I)_{\text{SMFT}}$ maps.

The HSOS/SMFT Stokes- $(V/I)_{\text{SMFT}}$ versus SDO/HMI B_{HMI} -distribution for all the magnetograms used for the cross-calibration is shown in Figure 2. The red calibration curve in the plot is the best least-square approximation of the distribution by a third-order polynomial

$$(V/I)_{\text{SMFT}} = C_0 + C_1 \times B_{\text{HMI}} + C_2 \times (B_{\text{HMI}})^2 + C_3 \times (B_{\text{HMI}})^3, \quad (6)$$

where $C_0 = -1.030 \times 10^{-4}$, $C_1 = 5.815 \times 10^{-5} \text{ G}^{-1}$, $C_2 = 2.743 \times 10^{-10} \text{ G}^{-2}$, $C_3 = -8.061 \times 10^{-12} \text{ G}^{-3}$. One can see in Figure 2 that the quasi-linear relationship holds for relatively weak magnetic fields, while Stokes- $(V/I)_{\text{SMFT}}$ starts to saturate for longitudinal magnetic field exceeding approximately 1000 G. The calibration constant C_{\parallel} in Equation 1 can be easily derived as $C_{\parallel} = 1/C_1$. We will refer to this constant as C_{SMFT} in the rest of the article. The value $C_1 = 5.815 \times 10^{-5} \text{ G}^{-1}$ for the linear relationship between $(V/I)_{\text{SMFT}}$ and B_{SMFT} is approximately 1.6 times smaller than the theoretical value obtained by Ai, Li, and Zhang (1982). However, this difference can be attributed to the different spectral lines used by HSOS/SMFT and SDO/HMI.

Figure 2 The logarithmic density of HSOS/SMFT Stokes- $(V/I)_{\text{SMFT}}$ versus SDO/HMI longitudinal magnetic field B_{HMI} distribution of ten randomly selected active regions observed between 2015 and 2018. The red calibration curve shows the best third-order-polynomial approximation (Equation 6) of the distribution.



Note that the use of the non-linear relationship between Stokes- (V/I) and B_{\parallel} has been proposed earlier. For example, Chae et al. (2007) have performed cross-calibration of *Narrow-band Filter Imager* (NFI) Stokes- (V/I) and the longitudinal magnetic field acquired by the *Spectropolarimeter* (SP) onboard *Hinode* (Kosugi et al., 2007). NFI is a filtergraph that observes Stokes- (V/I) at a single spectral point of Fe I 6173 Å line. There was a saturation of Stokes- (V/I) in the magnetic fields exceeding approximately 2000 G. Chae et al. (2007) proposed to use two different linear relationships to evaluate the longitudinal magnetic field from *Hinode*/NFI Stokes- (V/I) . A similar analysis was carried out by Moon et al. (2007) who proposed a method to eliminate saturation for magnetic-field measurements performed by *Michelson Doppler Imager* onboard the *Solar and Heliospheric Observatory* (SOHO/MDI; Scherrer et al., 1995). The authors used a second-order polynomial to approximate the strong-field part of the SOHO/MDI Stokes- (V/I) versus *Hinode*/SP B_{\parallel} -distribution.

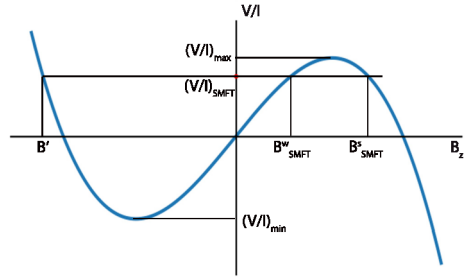
Figure 3 shows schematically the possible way of deriving longitudinal magnetic field from the measured Stokes- $(V/I)_{\text{SMFT}}$. As it follows from Equation 6, each value $(V/I)_{\text{SMFT}}$ lying between $(V/I)_{\text{min}}$ and $(V/I)_{\text{max}}$ corresponds to three values of B_{SMFT} : $B_{\text{SMFT}}^{\text{w}}$ (weak-field part of the calibration curve), $B_{\text{SMFT}}^{\text{s}}$ (strong-field part of the calibration curve), and B' . To get these values, we numerically solve the equation

$$C_0 + C_1 \times B_{\text{SMFT}} + C_2 \times (B_{\text{SMFT}})^2 + C_3 \times (B_{\text{SMFT}})^3 - (V/I)_{\text{SMFT}} = 0, \quad (7)$$

The real root of Equation 7 with the sign opposite to that of $(V/I)_{\text{SMFT}}$ corresponds to B' and must be rejected. The other two roots are $B_{\text{SMFT}}^{\text{w}}$ and $B_{\text{SMFT}}^{\text{s}}$ (the latter has a higher absolute value). One of the weak points of the algorithm are the cutoff values labeled with $(V/I)_{\text{max}}$ for positive and with $(V/I)_{\text{min}}$ for negative $(V/I)_{\text{SMFT}}$ in Figure 3. Apparently, Stokes- $(V/I)_{\text{SMFT}}$ values exceeding $(V/I)_{\text{max}}$ have to be replaced by $(V/I)_{\text{max}}$. Stokes- $(V/I)_{\text{SMFT}}$ values that are less than $(V/I)_{\text{min}}$ must be replaced by $(V/I)_{\text{min}}$ as well. One should keep in mind that this artificial procedure may result in unrealistic morphology of the derived magnetic-field maps.

The next step of our method is to figure out in which part of the calibration curve our particular pixel lies, i.e. whether this value of Stokes- $(V/I)_{\text{SMFT}}$ in the given pixel corresponds to the weak or the strong magnetic field. To answer this question, we propose to use the information on continuum intensity at the pixel. Norton and Gilman (2004) have shown that there is a direct relationship between continuum intensity and magnetic-field strength. Hence, we can readily use the observable Stokes- I_{SMFT} as a proxy for the continuum intensity to figure out which part of the calibration curve to use to derive the value of the magnetic

Figure 3 A schematic illustration of the magnetic-field derivation using the third-order-polynomial (Equation 6). The measured Stokes- V/I values $(V/I)_{SMFT}$ correspond to three possible values of the longitudinal magnetic field.



field from Stokes- $(V/I)_{SMFT}$: the continuum intensity or Stokes- I_{SMFT} in the strong magnetic field regions is sufficiently lower than that in the weak magnetic field or quiet-Sun areas (cf. Chae et al., 2007).

A straight-forward choice of the threshold value of Stokes- I_t for separating pixels into the two subsets of strong and weak magnetic field might be inappropriate: due to the noise in the Stokes- I_{SMFT} maps, two adjacent pixels with nearly the same value of the longitudinal magnetic field could be attributed to different parts of the calibration curve (either weak- or strong-field parts). As a result, sudden discontinuities of B_{SMFT} might be observed in the derived map of the longitudinal magnetic field. Another option is to set two thresholds I_s and I_w ($I_s < I_w$) such that pixels with $I_{SMFT} < I_s$ definitely belong to the strong-field subset and pixels with $I_{SMFT} > I_w$ definitely belong to the weak-field subset. In such a case, the magnetic field in pixels with $I_s < I_{SMFT} < I_w$, i.e. in pixels with some intermediate magnetic fields, has to be derived, for example, by interpolation between the strong and weak magnetic fields. We have tested both approaches and found no advantages of one over the other. Both of them may add artificial non-physical structures in the magnetic-field maps. Hence, we use a single threshold I_t to distinguish between strong and weak magnetic fields. If the required cadence of the data is not high enough, manual choice of the threshold value I_t by an observer is acceptable.

The modified algorithm for deriving B_{SMFT} from Stokes- $(V/I)_{SMFT}$ can be summarized as follows:

- i) Separate all pixels into two sets of strong and weak magnetic-field pixels by applying threshold I_t to Stokes- I_{SMFT} map.
- ii) For each pixel of the magnetogram, calculate the roots of the polynomial (Equation 7). If the $(V/I)_{SMFT}$ value in the pixel is greater than $(V/I)_{max}$ (as defined in Figure 3) set $(V/I)_{SMFT} = (V/I)_{max}$. Similarly, pixels with $(V/I)_{SMFT}$ less than $(V/I)_{min}$ have to be replaced with $(V/I)_{min}$.
- iii) Set the magnetic-field value in the pixel to a corresponding root of the polynomial: weak-field pixels (as defined in step i) correspond to the root with the lower absolute value.
- iv) Smooth the magnetogram to eliminate possible discontinuities near pixels with Stokes- $I_{SMFT} = I_t$.

Figure 4 demonstrates Stokes- $(V/I)_{SMFT}$ (Panel a), B_{SMFT} derived by the proposed algorithm (Panel b), and B_{HMI} (Panel c) of the unipolar NOAA Active Region 12670. A clear saturation of $(V/I)_{SMFT}$ in the active region’s umbra is visible. The slices of the maps are shown in Figure 4d. Saturation in the umbra was eliminated in the final map of B_{SMFT} . The maximum B_{SMFT} -value inside umbra is about 2200 G which is comparable to the value derived by SDO/HMI. For comparison, B_{SMFT} derived from $(V/I)_{SMFT}$ by the linear rela-

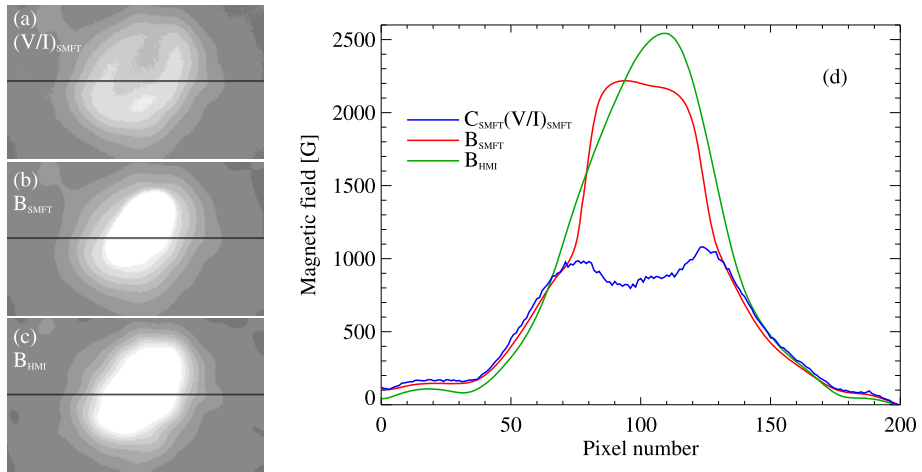


Figure 4 Maps of Stokes- $(V/I)_{SMFT}$ (a), magnetic field B_{SMFT} derived by the proposed algorithm (b), and smoothed SDO/HMI magnetic field B_{HMI} (c) of NOAA Active Region 12670 observed on 17 August 2017. The field-of-view is $50'' \times 35''$. The maps are scaled from -1500 G (black) to 1500 G (white). Panel d demonstrates slices of the maps shown in Panels a–c. The positions of the slices are denoted by horizontal black lines in Panels a–c.

relationship (Equation 1) ($C_{\parallel} = C_{SMFT}$) would yield approximately 2.7 times lower values of the magnetic field inside the umbra.

To verify the consistency of our methodology, we derived the longitudinal magnetic field B_{HMI}^{wf} from SDO/HMI Stokes- $(V/I)_{HMI}$ measurements acquired at a single wavelength. To do so, we performed a cross-calibration between $(V/I)_{HMI}$ and B_{HMI} to obtain coefficients in Equation 6 suitable for the SDO/HMI instrument. Then the B_{HMI}^{wf} map was evaluated using the algorithm described above. Indeed, in contrast to the ground-based HSOS/SMFT, the cross-calibration of such a reduced SDO/HMI Stokes- $(V/I)_{HMI}$ at a single spectral-line point and the SDO/HMI- B_{HMI} obtained by the VFISV code is free from all errors caused by different seeing, spatial resolution, etc.

SDO/HMI Stokes- $(V/I)_{HMI}$ maps were derived from the observations in the fourth filter position. The data on NOAA Active Region 12674 acquired on 5 September 2017 at 05:48 TAI were used. SDO/HMI Stokes- $(V/I)_{HMI}$ versus SDO/HMI- B_{HMI} is shown in Figure 5a. The same saturation effect in strong magnetic fields as in Figure 2 can be seen. The scatter plot of the derived SDO/HMI longitudinal magnetic field B_{HMI}^{wf} versus SDO/HMI- B_{HMI} is shown in Figure 5b. One can see a good consistency between the data series. The linear correlation coefficient between B_{HMI}^{wf} and B_{HMI} is 0.96.

Figure 6 shows B_{HMI} , $(V/I)_{HMI}$ and B_{HMI}^{wf} maps of NOAA Active Region 12674 in Panels a, b, and c, respectively. One can see that the method compensates for the saturation effect within the stronger leading and the weaker following sunspots in the active region.

4. Results

To illustrate the performance of the method, we derived longitudinal magnetic field B_{SMFT} of four active regions (Figure 7, second row from the top). Stokes- $(V/I)_{SMFT}$ acquired by HSOS/SMFT and co-temporary SDO/HMI magnetograms of the same active regions are

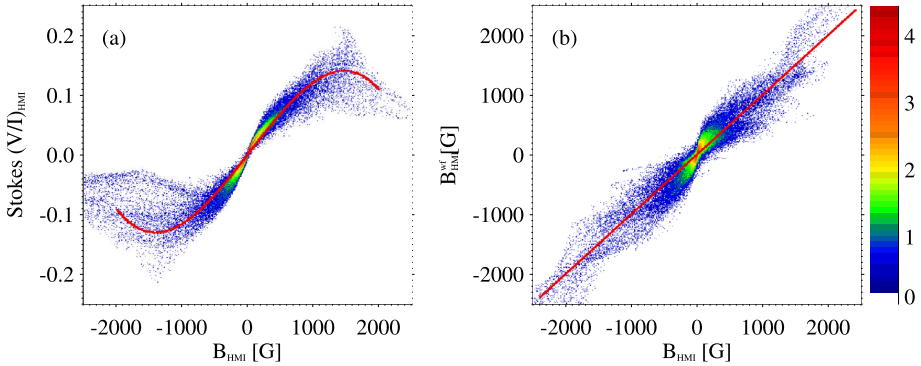


Figure 5 The logarithmic density of $(V/I)_{\text{HMI}}$ versus B_{HMI} and of $B_{\text{HMI}}^{\text{wf}}$ versus B_{HMI} distributions of NOAA Active Region 12674 observed on 5 September 2017 at 05:48 TAI. B_{HMI} is the longitudinal magnetic field derived by the proposed algorithm using Stokes- $(V/I)_{\text{HMI}}$ measurements at a single wavelength point. The red curve in Panel **a** is the best third-order-polynomial fit of the distribution. Red curve in Panel **b** shows $y = x$ relationship.

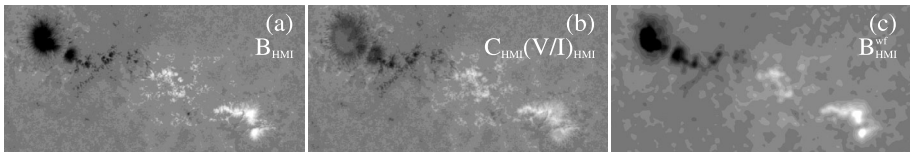


Figure 6 Maps of the longitudinal magnetic field B_{HMI} (**a**), Stokes $C_{\text{HMI}}(V/I)_{\text{HMI}}$ (**b**), and $B_{\text{HMI}}^{\text{wf}}$ (**c**) of NOAA Active Region 12674 acquired by SDO/HMI on 5 September 2017 at 05:48 TAI. $(B)_{\text{HMI}}^{\text{wf}}$ is the longitudinal magnetic field derived by the proposed algorithm using Stokes- $(V/I)_{\text{HMI}}$ measurements at a single wavelength point. The field-of-view is $350'' \times 175''$. The magnetic-field values over the magnetograms are scaled from -2000 G (black) to 2000 G (white). The constant C_{HMI} is the linear calibration coefficient between B_{HMI} and Stokes- $(V/I)_{\text{HMI}}$ (cf. Figure 4).

shown for comparison in the first and third rows (from the top) of Figure 7. To derive, B_{SMFT} the intensity threshold was set to $I_t = 0.5I_c$, where I_c is Stokes- I_{SMFT} of the quiet-Sun intensity.

One can see that the saturation in Stokes- $(V/I)_{\text{SMFT}}$ is observed within the strong magnetic-field concentrations (see the maps in the top row of Figure 7). At the same time, both the HSOS/SMFT magnetograms derived using the proposed algorithm, and the SDO/HMI magnetograms are free of this effect. The algorithm allows us to reconstruct the morphological structure of an active region. For example, the leading negative polarity of NOAA Active Region 12470 in the $(V/I)_{\text{SMFT}}$ map (top row) represents a horseshoe-shaped structure. In the B_{SMFT} map, this magnetic feature is a well-defined strong sunspot.

The difference maps between B_{HMI} and $C_{\text{SMFT}}(V/I)_{\text{SMFT}}$ are shown in the fourth (from the top) row of Figure 7. A significant difference is observed in the sunspot umbrae implying considerable underestimation of the magnetic-field strength. On the other hand, in the sunspot umbrae the difference maps between B_{HMI} and B_{SMFT} (the bottom row in Figure 7) in most cases show the sign opposite to that of $B_{\text{HMI}} - C_{\text{SMFT}}(V/I)_{\text{SMFT}}$. Consequently, the proposed algorithm often overestimates the magnetic-field magnitude in areas with strong magnetic fields. Besides that, the artifacts of the algorithm (e.g. concentric rings around the sunspot penumbra) can be revealed in the difference $B_{\text{HMI}} - B_{\text{SMFT}}$ maps. These artifacts

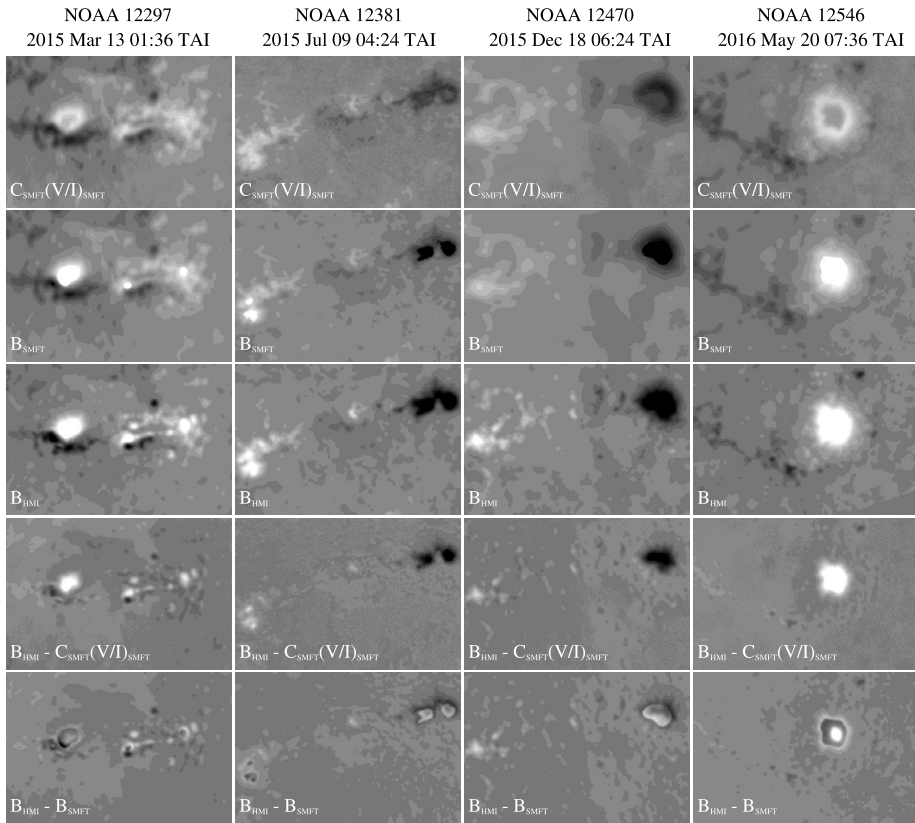


Figure 7 Maps (from top to bottom) of Stokes- $C_{SMFT}(V/I)_{SMFT}$, longitudinal magnetic field B_{SMFT} derived using the proposed algorithm, smoothed SDO/HMI longitudinal magnetic field B_{HMI} , the difference $B_{HMI} - C_{SMFT}(V/I)_{SMFT}$, and the difference $B_{HMI} - B_{SMFT}$ for four NOAA Active Regions 12297, 12381, 12470, and 12546 (from left to right). The field-of-view of the maps is $230'' \times 155''$. The magnetic-field values are scaled from -1500 G (black) to 1500 G (white).

Table 1 The standard deviation [G] of the difference maps shown in the bottom rows of Figure 7.

	NOAA AR			
	12297	12381	12470	12546
$B_{HMI} - C_{SMFT}(V/I)_{SMFT}$	138	125	135	255
$B_{HMI} - B_{SMFT}$	92	71	84	100

could be probably diminished by varying the threshold I_t for each active region individually.

The standard deviation of the difference maps shown in the bottom rows of Figure 7 is listed in Table 1. One can see that the standard deviation of $B_{HMI} - C_{SMFT}(V/I)_{SMFT}$ maps is approximately two times higher than that of $B_{HMI} - B_{SMFT}$ maps. Consequently, in general the proposed algorithm yields better estimation of the longitudinal magnetic field than the traditional weak-field approximation.

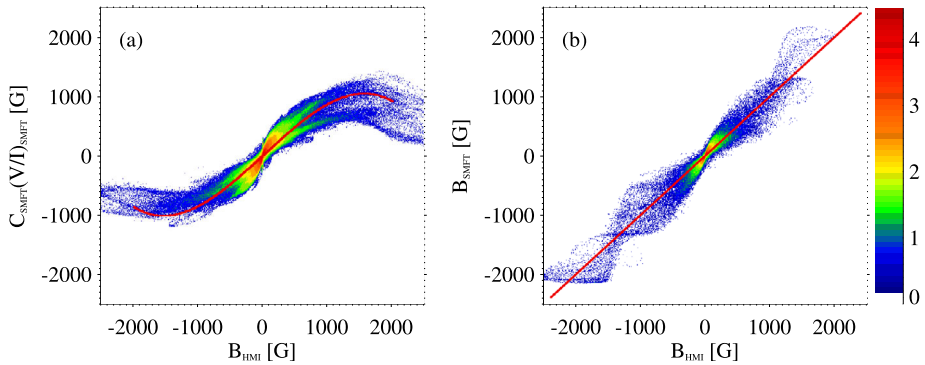


Figure 8 The logarithmic density of $C_{SMFT}(V/I)_{SMFT}$ versus B_{HMI} and B_{SMFT} versus B_{HMI} distributions for the four active regions shown in Figure 7. Red curve in Panel **a** is the best third-order-polynomial fit of the distribution. The red curve in Panel **b** shows $y = x$ relationship. The quasi-linear relationship in Panel **b** holds for magnetic fields as high as 2000 G.

The distributions $C_{SMFT}(V/I)_{SMFT}$ versus B_{HMI} and B_{SMFT} versus B_{HMI} for four selected active regions (Figure 7) are shown in Figure 8. In contrast to Figures 2 and 8a, a quasi-linear relationship holds for magnetic fields as high as 2000 G in the right panel of Figure 8.

The efficiency of the algorithm can also be evaluated by calculating the correlation coefficient between B_{HMI} and the magnetic-field maps derived from HSOS/SMFT observations. However, the distributions in Figure 8 suggest that the data points exhibiting weak-field values are the most numerous. These points may affect the correlation coefficient significantly. To get more reliable values for Pearson's R we split the points in both panels of Figure 8 into ten subsets according to their B_{HMI} -values. In each subset, 2000 points were randomly selected. Linear correlation coefficients were calculated for all the selected points that formed equally distributed $C_{SMFT}(V/I)_{SMFT}$ versus B_{HMI} and B_{SMFT} versus B_{HMI} relationships. This procedure yields Pearson's $R = 0.66$ for $C_{SMFT}(V/I)_{SMFT}$ versus B_{HMI} distribution (Figure 8a) and Pearson's $R = 0.99$ for B_{SMFT} versus B_{HMI} (Figure 8b).

Finally, Figure 9 shows transverse magnetic field in NOAA Active Region 12670 that was inferred from the observed HSOS/SMFT Stokes- Q and $-U$. To perform the 180-degree disambiguation, the transverse magnetic-field vector in each pixel of the magnetogram was co-aligned with the direction of the transverse potential magnetic field. The potential field was calculated from the saturated longitudinal magnetic field (Figure 4a) for green arrows and from de-saturated longitudinal magnetic field (Figure 4b) for red arrows. As expected, saturation prevents the transverse magnetic field from being oriented in an incorrect direction inside umbral regions.

5. Summary

We have used SDO/HMI longitudinal magnetic-field data on several active regions to perform a non-linear cross-calibration of HSOS/SMFT Stokes- $(V/I)_{SMFT}$. The essential element of the method is the use of non-linear relationships between Stokes- (V/I) and the longitudinal magnetic field. Due to certain procedures (for example, setting the limit for $(V/I)_{SMFT} = (V/I)_{max}$ if $(V/I)_{SMFT}$ exceeds $(V/I)_{max}$), the method is not suitable for precise reconstruction of the spatial structure of the longitudinal magnetic field from the

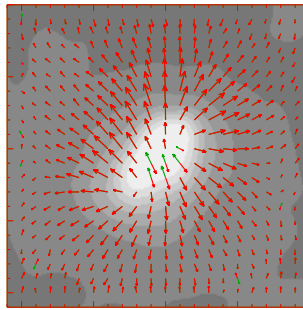


Figure 9 Longitudinal magnetic field B_{SMFT} in NOAA Active Region 12670 acquired by HSOS/SMFT on 17 August 2017 at about 05:18 UT. Red and green arrows point out the direction of the transverse magnetic field for different data on longitudinal magnetic field used for the 180-degree disambiguation (see text). The field-of-view is $45'' \times 45''$. The magnetogram is scaled from -2000 G (black) to 2000 G (white).

Stokes- $(V/I)_{\text{SMFT}}$. However, the main advantage of the method is the elimination of saturation inside strong magnetic-field areas such as in sunspot umbrae. This feature of the method is important for resolving of 180-degree disambiguation for the transverse magnetic field and the subsequent calculation of the electric current density. Thus, the method might be applied to the archive of HSOS/SMFT vector magnetic-field observations in order to improve the evaluation of electric currents and current helicity in solar active regions since 1987, which can be implemented in forthcoming studies.

Acknowledgments We are sincerely grateful to the anonymous reviewer whose comments helped us reconsider the method and to significantly improve the article. The work is supported by the joint cost-shared RFBR of Russia and NNSF of China grant, Russian Fund for Basic Research numbers 17-52-53203 and 19-52-53045, also grants 11427901, 10921303, 11673033, U1731113, 11611530679, 11573037, 11703042, 11911530089, 12073040, and 12073041 of the National Natural Science Foundation of China. S. Yang acknowledges support by grants 11427901, 10921303, 12073040, 11673033, U1731113, 11611530679, and 11573037 of the National Natural Science Foundation of China and grants no. XDB09040200, XDA04061002, XDA15010700 of the Strategic Priority Research Program of Chinese Academy of Sciences and the Youth Innovation Promotion Association of CAS (2019059). Theoretical calculations in Section 2 were performed with the support by the Russian Science Foundation, Project 18-12-00131. A.A. Plotnikov, A.S. Kutsenko, and K.M. Kuzanyan would like to thank the Huairou Solar Observing station of NAOC for their hospitality during their visits to China.

Declarations

Disclosure of Potential Conflicts of Interest The authors declare that they have no conflicts of interest.

References

- Ai, G.-X.: 1987, Solar magnetic field telescope. *Pub. Beijing Astron. Obs.* **9**, 27. [ADS](#).
- Ai, G.-X., Li, W., Zhang, H.-Q.: 1982, FeI λ 5324.19 A line forms in the solar magnetic field and the theoretical calibration of the solar magnetic field telescope. *Acta Astron. Sin.* **23**, 39. [ADS](#).
- Bai, X.Y., Deng, Y.Y., Su, J.T.: 2013, Calibration of vector magnetograms with the chromospheric Mg b_2 line. *Solar Phys.* **282**, 405. [DOI](#). [ADS](#).
- Bai, X.Y., Deng, Y.Y., Teng, F., Su, J.T., Mao, X.J., Wang, G.P.: 2014, Improved magnetogram calibration of Solar Magnetic Field Telescope and its comparison with the Helioseismic and Magnetic Imager. *Mon. Not. Roy. Astron. Soc.* **445**, 49. [DOI](#). [ADS](#).
- Bellot Rubio, L.: 2003, *Inversion of Stokes Profiles with SIR (Stokes Inversion on Response Functions)*, Kiepenheuer Institut für Sonnenphysik, Freiburg.

- Bobra, M.G., Sun, X., Hoeksema, J.T., Turmon, M., Liu, Y., Hayashi, K., Barnes, G., Leka, K.D.: 2014, The Helioseismic and Magnetic Imager (HMI) vector magnetic field pipeline: SHARPs – Space-weather HMI Active Region Patches. *Solar Phys.* **289**, 3549. DOI. ADS.
- Borrero, J.M., Tomczyk, S., Kubo, M., Socas-Navarro, H., Schou, J., Couvidat, S., Bogart, R.: 2011, VFISV: Very Fast Inversion of the Stokes Vector for the Helioseismic and Magnetic Imager. *Solar Phys.* **273**, 267. DOI. ADS.
- Canfield, R.C., de La Beaujardiere, J.-F., Fan, Y., Leka, K.D., McClymont, A.N., Metcalf, T.R., Mickey, D.L., Wuelser, J.-P., Lites, B.W.: 1993, The morphology of flare phenomena, magnetic fields, and electric currents in active regions. I. Introduction and methods. *Astrophys. J.* **411**, 362. DOI. ADS.
- Chae, J., Moon, Y.-J., Park, Y.-D., Ichimoto, K., Sakurai, T., Suematsu, Y., Tsuneta, S., Katsukawa, Y., Shimizu, T., Shine, R.A., Tarbell, T.D., Title, A.M., Lites, B., Kubo, M., Nagata, S., Yokoyama, T.: 2007, Initial results on line-of-sight field calibrations of SP/NFI data taken by SOT/Hinode. *Pub. Astron. Soc. Japan* **59**, S619. DOI. ADS.
- Cobo, B., del Toro Iniesta, J.C.: 1992, Inversion of Stokes profiles. *Astrophys. J.* **398**, 375. DOI.
- del Toro Iniesta, J.C.: 2003, *Introduction to Spectropolarimetry*, Cambridge University Press, Cambridge. DOI. ADS.
- del Toro Iniesta, J.C., Ruiz Cobo, B.: 2016, Inversion of the radiative transfer equation for polarized light. *Liv. Rev. Solar Phys.* **13**, 4. DOI. ADS.
- Fontenla, J.M., Avrett, E.H., Loeser, R.: 1993, Energy balance in the solar transition region. III. Helium emission in hydrostatic, constant-abundance models with diffusion. *Astrophys. J.* **406**, 319. DOI. ADS.
- Guo, J., Bai, X., Deng, Y., Liu, H., Lin, J., Su, J., Yang, X., Ji, K.: 2020, A non-linear magnetic field calibration method for filter-based magnetographs by multilayer perceptron. *Solar Phys.* **295**, 5. DOI. ADS.
- Hoeksema, J.T., Liu, Y., Hayashi, K., Sun, X., Schou, J., Couvidat, S., Norton, A., Bobra, M., Centeno, R., Leka, K.D., Barnes, G., Turmon, M.: 2014, The Helioseismic and Magnetic Imager (HMI) vector magnetic field pipeline: overview and performance. *Solar Phys.* **289**, 3483. DOI. ADS.
- Jefferies, J., Lites, B.W., Skumanich, A.: 1989, Transfer of line radiation in a magnetic field. *Astrophys. J.* **343**, 920. DOI. ADS.
- Kosugi, T., Matsuzaki, K., Sakao, T., Shimizu, T., Sone, Y., Tachikawa, S., Hashimoto, T., Minesugi, K., Ohnishi, A., Yamada, T., Tsuneta, S., Hara, H., Ichimoto, K., Suematsu, Y., Shimojo, M., Watanabe, T., Shimada, S., David, J.M., Hill, L.D., Owens, J.K., Title, A.M., Culhane, J.L., Harra, L.K., Doschek, G.A., Golub, L.: 2007, The Hinode (Solar-B) mission: an overview. *Solar Phys.* **243**, 3. DOI. ADS.
- Landi Degl'Innocenti, E., Landi Degl'Innocenti, M.: 1973, A perturbative solution of the transfer equations for the Stokes parameters in a magnetic field. *Solar Phys.* **31**, 299. DOI. ADS.
- Landi Degl'Innocenti, E., Landolfi, M.: 2004, *Polarization in Spectral Lines* **307**, Kluwer, Dordrecht. DOI. ADS.
- Maltby, P., Avrett, E.H., Carlsson, M., Kjeldseth-Moe, O., Kurucz, R.L., Loeser, R.: 1986, A new sunspot umbral model and its variation with the solar cycle. *Astrophys. J.* **306**, 284. DOI. ADS.
- Metcalf, T.R.: 1994, Resolving the 180-degree ambiguity in vector magnetic field measurements: the 'minimum' energy solution. *Solar Phys.* **155**, 235. DOI. ADS.
- Moon, Y.-J., Kim, Y.-H., Park, Y.-D., Ichimoto, K., Sakurai, T., Chae, J., Cho, K.S., Bong, S., Suematsu, Y., Tsuneta, S., Katsukawa, Y., Shimojo, M., Shimizu, T., Shine, R.A., Tarbell, T.D., Title, A.M., Lites, B., Kubo, M., Nagata, S., Yokoyama, T.: 2007, Hinode SP vector magnetogram of AR10930 and its cross-comparison with MDI. *Pub. Astron. Soc. Japan* **59**, S625. DOI. ADS.
- Norton, A.A., Gilman, P.A.: 2004, Magnetic field-minimum intensity correlation in sunspots: a tool for solar dynamo diagnostics. *Astrophys. J.* **603**, 348. DOI. ADS.
- Rachkovsky, D.N.: 1962, Magnetic rotation effects in spectral lines. *Izv. Krym. Astrofiz. Obs.* **28**, 259. ADS.
- Rees, D.E., Semel, M.D.: 1979, Line formation in an unresolved magnetic element: a test of the centre of gravity method. *Astron. Astrophys.* **74**, 1. ADS.
- Sakurai, T., Ichimoto, K., Nishino, Y., Shinoda, K., Noguchi, M., Hiei, E., Li, T., He, F., Mao, W., Lu, H., Ai, G., Zhao, Z., Kawakami, S., Chae, J.-C.: 1995, Solar Flare Telescope at Mitaka. *Pub. Astron. Soc. Japan* **47**, 81. ADS.
- Scherrer, P.H., Bogart, R.S., Bush, R.I., Hoeksema, J.T., Kosovichev, A.G., Schou, J., Rosenberg, W., Springer, L., Tarbell, T.D., Title, A., Wolfson, C.J., Zayer, I., MDI Engineering Team: 1995, The solar oscillations investigation – Michelson Doppler Imager. *Solar Phys.* **162**, 129. DOI. ADS.
- Scherrer, P.H., Schou, J., Bush, R.I., Kosovichev, A.G., Bogart, R.S., Hoeksema, J.T., Liu, Y., Duvall, T.L., Zhao, J., Title, A.M., Schrijver, C.J., Tarbell, T.D., Tomczyk, S.: 2012, The Helioseismic and Magnetic Imager (HMI) Investigation for the Solar Dynamics Observatory (SDO). *Solar Phys.* **275**, 207. DOI. ADS.
- Schou, J., Scherrer, P.H., Bush, R.I., Wachter, R., Couvidat, S., Rabello-Soares, M.C., Bogart, R.S., Hoeksema, J.T., Liu, Y., Duvall, T.L., Akin, D.J., Allard, B.A., Miles, J.W., Rairden, R., Shine, R.A., Tarbell, T.D., Title, A.M., Wolfson, C.J., Elmore, D.F., Norton, A.A., Tomczyk, S.: 2012, Design and ground

- calibration of the Helioseismic and Magnetic Imager (HMI) instrument on the Solar Dynamics Observatory (SDO). *Solar Phys.* **275**, 229. [DOI](#). [ADS](#).
- Su, J.-T., Zhang, H.-Q.: 2004, Calibration of vector magnetogram with the nonlinear least-squares fitting technique. *Chin. J. Astron. Astrophys.* **4**, 365. [DOI](#). [ADS](#).
- Unno, W.: 1956, Line formation of a normal Zeeman triplet. *Pub. Astron. Soc. Japan* **8**, 108. [ADS](#).
- Zhang, H.: 2019, From polarimetry to helicity: studies of solar magnetic fields at the Huairou Solar Observing Station. *Sci. China Ser. G, Phys. Mech. Astron.* **62**, 999601. [DOI](#). [ADS](#).
- Zhang, H., Sakurai, T., Pevtsov, A., Gao, Y., Xu, H., Sokoloff, D.D., Kuzanyan, K.: 2010, A new dynamo pattern revealed by solar helical magnetic fields. *Mon. Not. Roy. Astron. Soc.* **402**, L30. [DOI](#). [ADS](#).

Publisher's Note Springer Nature remains neutral with regard to jurisdictional claims in published maps and institutional affiliations.